Turkish Online Journal of Qualitative Inquiry (TOJQI)
Volume 09, Issue 4, December 2018: 459-472
DOI: 10.53555/tojqi.v9i4.10592

Research Article

Biological Molecules Based Nano Composites Synthesization Using De-Oxy Ribo Nucleic Acid

Deepa S[1*], Sasikumar P[2]

Abstract

Learning the nanocrystal formation process is a requirement for comprehending all fundamental aspects of three-dimensional confining in semiconductor materials. The most crucial details to be gleaned from growth based include the nanocrystals' dimensions, surface area, stoichiometry, structural, and interface design. Nanocrystal growth is intended to occur solely through thermodynamic deposition, followed by propagation in the immediate vicinity of the nanocluster, with no interplay between them. The proposed synthesization procedure utilizes De-oxy Ribo Nucleic Acid (DRNA) based processing for the preparation of nano composites with Zinc oxide. Repeated potential cycling process in acidic media is also performed for this catalyst and found excellent stability with only few drops in the wave potential. The strong fibrous framework of ZnO and its efficient functionalization process are credited with contributing to the excellent behaviour of the ZnO-DNRA catalyst. In the field of nanomedicine, it is very desirable for nanomaterials to have improved magnetic (i.e., paramagnetic or ultra-paramagnetic) characteristics, high electric conductance, and very well reactivity.

Keywords: Nano composites, DRNA, Zinc oxide, TEM, EDRA, bandgap and nano-crystal.

Introduction

Synthesis of nanocrystals with regulated size distribution is of interest charged to their quantum confinement effects, luminous characteristics, and other physical and chemical features. Optoelectronic devices, solar energy conversion molecules, intracellular imaging, and trace detecting are just a few of the many uses [1] . A key characteristic of nanocrystals is the quantum size phenomenon, which causes charge carriers to be spatially enclosed inside the nanocrystal. This operation allows us to change the medium's Ultraviolet light, visual, IRs, and mid-IRs source. For instance, the semiconducting nanoparticle band gap may be tuned across a broad range of wavelengths by increasing the proper size. The fluorescence intensity spectrum of nanoparticles may be continuously altered by changing particle diameter, and a particular occurrence can be used to stimulate all various nanocrystals [2-5].

Among the most significant II-VI semiconductor compounds with outstanding optical characteristics is ZnO. It is a direct material with a bandgaps of 3.37 eV at 300 K. A lot of work has gone into synthesizing and studying ZnO nanoparticles and quantum dots. Synthesis of highly micro-particles ZnO nanocrystal is possible by size-restricted growth techniques. One approach to enforcing the size constraint is to include organic surface-capping components in the mixture. Tunable electroluminescent devices and low-voltage displays are now possible thanks to this straightforward preparation method. When the N and crystallites' diameters are similar to the exciton Bohr radius, which corresponds to an expansion of the energy imbalance as size lowers, there is a considerable

[1] Assistant professor, Department of Physics, Government College of Engineering, Salem.
Email: deepasasi1984@gmail.com
[2] Professor, School of Computing Science and Engineering, Galgotias University, Greater Noida, Uttar Pradesh. sasi.mca@gmail.com

shift in the characteristics. The chemical process is a straightforward and cost-effective way to produce Nanoparticles.

DRNA is employed as a bio pattern to build inorganic quantum-restricted nanoparticles and naturally non-biological fundamental materials into larger nano-composites [6-8] because of its metabolic durability and unique design. The convergence of nanotechnology, biology, and medicines should boost cell genetics and biotechnology. Proteins may be used as templates to synthesize inorganic nanomaterials with well-defined construction and regulated proportions. We used DRNA as a stabilizing agent in the coprecipitation to create Nanoparticles.

The DRNA that contains the genetic code in all living things is the most significant and well-known biopolymer that man is aware of. DRNA, "the atom of life," has attracted experts in science and technology for 20 years. DRNA molecules have recently been mentioned as a possible database medium. DRNA memory, which uses DRNA molecules and DRNA processes for data processing, is a high-capacity, high-density memory. DRNA is being used in nanotechnology. A new discipline known as nanobiotechnology was created by linking biology with nanomaterials. Quantum dots, quantum wires, nanostructured materials, iron oxides, and sulphur dioxide are examples of inorganic quantum-restricted nanostructures that may be created using DRNA.

DRNA may guide the polymerization of conductive polymers. Polypyrrole and polyaniline are produced on Template DRNA by interfacing with its Si-immobilized framework. It is possible to manufacture high-density carbon composite nanostructures on a Si substrate using this technology [9]. These nanotubes would have a preset arrangement and configuration.

Materials and Methodology

All chemicals, as well as DRNA powder, were bought from businesses (SRI, Merck). We employed DRNA wrapping methods to adjust particle size. 0.10 M Zinc Acetate and 0.10 M Nacl are added drop by drop to 0.01 wt% DRNA room temperature solution at 1 Oml per hour using a mechanical stirrer. Additive rate, reaction temperature, & catalyst loading are key in synthesis. The white precipitate is filtered and washed to eliminate mother compounds. Filtered, dried in a 60° C hot air oven, and then crushed into fine powdered.

Synthesis Method

There are two methods used in nano production. The first approach involves using mechanical, biochemical, or other sorts of energies to first decompose large amounts of material into smaller pieces (top-down). Creating the material from molecules or atoms particles by chemical processes while enabling the preceding atoms to expand is an alternate method (bottom-up). According to many studies [10-15] both methodologies may be implemented in a vacuum, supercritical fluids, liquid, solid, or as states. Most manufacturers want the ability to regulate the following three factors: a) particle density; b) particle morphology; and c) volume fraction. d) the makeup of the nanomaterials; e) the degree of crystallization [16]

Numerous studies have been done on the production of nanostructured metal oxides and their mixtures using a variety of processes, such as **SolGel [17],** self-assembly **[18],** chemical deposition **[19],** emulsion route **[20],** vapor deposition transport [**21**], reactive sputtering **[22],** and spray

Co-precipitation technique

The co-precipitation approach is the most often used synthetic strategy. The current work's study of metal oxides and metal oxide composites uses a chemical co-precipitation approach to create all of the materials. Mixed powder with an adequate stoichiometric ratio, impurity, homogenization, and regulated appearance may be obtained with the help of inorganic salt-based co-precipitating agents. [23] pH, integration rates, temperatures, and focus must be controlled during processing.

This process produces metal oxide nanoparticles and composites. The size of nanoparticles is controlled by many factors, each of which is tuned individually. It has been shown that temperature, pH, duration, speed of stirring, and the rate at which chemicals are added is crucial in regulating the

size of the nanoparticles. In this experiment, particle size and shape were dependent on initial reagent molarity. To create the metal oxide nanoparticles, four distinct reagent molar levels are used.

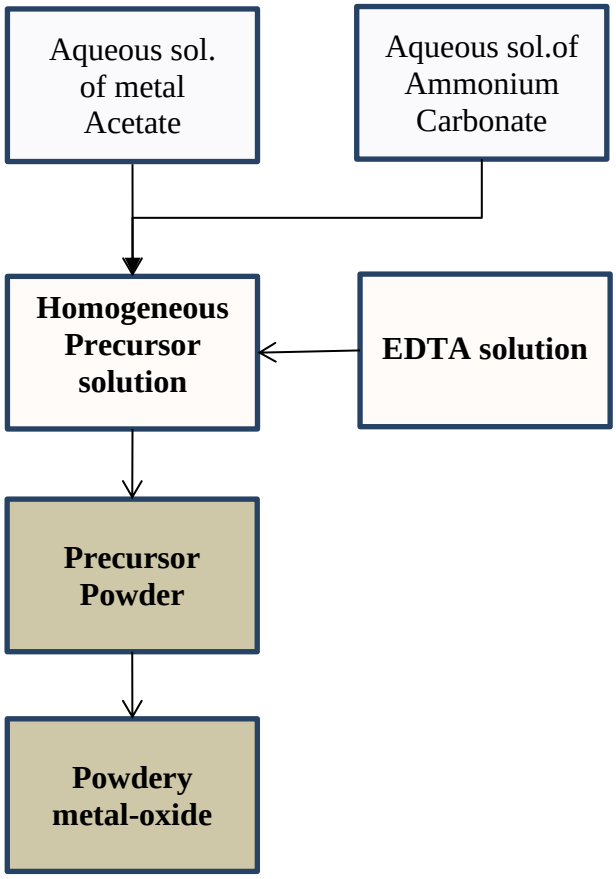

Figure 1: Flow chart of synthesis process

Sample preparation

Methods

The chemical co-precipitation approach is used in the current investigation to prepare the samples. The samples are nanoparticles of zinc oxide, magnesium oxide, and nanocomposites of (ZnO/MgO) and (ZnO/CdO). The chemicals utilized in this project are all of the AR grades. Without additional processing, the chemicals are utilized directly after being obtained from MERCK. Nanoparticle production uses freshly generated aqueous-phase mixtures. To investigate the role of reagent molarity in regulating particle size and shape, reagent molar mass was changed from 0.05M to 0.2M in 0.05M increments.

Synthesis of ZnO nanoparticles

In this study, Zinc Acetate and Ammonia Solution were used to make nanostructure Zinc Oxide particles. Double-distilled water was used to create each solution. Using a burette, the 0.05M concentrations of Zinc Acetate and Ammonium Carbonate were concurrently dripped at a rate of 1 mol/hr into a 0.01 molar solution of EDTA while being stirred continuously. The white bicarbonate precipitation was taken from the reaction medium and subsequently washed with ethanol before being treated with distilled water to eliminate impurities and chemical residues. The wet precipitation was ground into a fine powder after being allowed to spontaneously dry. This produced the metal bicarbonate predecessor.

TGA study of carbonate precipitate demonstrated a rapid weight loss between 450°C and 500°C. When this metal carbonate is heated to the necessary temperature, it breaks down to generate metal

oxide. For solutions of Zinc Acetate and Ammonium Carbonate that are 0.1 Mg, 0.15 Mg, and 0.2 Mg, the synthesizing procedure is repeated. The specimens of zinc oxides that were collected in this sequence are designated Zl, Z2, Z3, and Z4, and will be referenced by these names from this point forward.

Synthesis of MgO nanoparticles

By using the precipitation process, magnesium oxide nanoparticles were also created. 0.05 M solutions of Magnesium Acetate and Ammonia Solution were used to make Mgo nano material. The EDTAs level were set at 0.01 M, and the NaHo level at 1 M.

All concentrations were produced in distilled water, and Magnesium Acetate• and 0.1 molar Ammonium Carbonate were progressively drop into 0.01m EDT A under continual magnetic stirring. EDTA and Sodium Hydroxide were tuned to balance give way and element size.[24] The rate of stirring and drop period affect the size of nanoparticles. These variables were each tuned separately. The final result went through filtration, drying, and fine grinding in an agate mortar. The pulverized powder was annealed for three hours at 500°C to produce oxide particles. Magnesium acetate and ammonia solution are used in 0.1, 0.15, and 0.2 molar amounts, respectively. The specimens of mg oxides that were obtained in this sequence are designated M1, M2, M3, and M4, respectively, and will be referenced by these names from this point forward.

Synthesis of (ZnO/MgO) - nanocomposite

Co-precipitating Zinc Oxide and Magnesium Oxide carbonates yield a solid solution. Zinc Solutions of acetate and mg oxalate were diluted and combined with 0.2M ammonium hydroxide for a reaction. The EDTAs and Nacl ratios were maintained throughout. 3 solutions—Zinc acetate, Mg acetic acid, and Potassium Bicarbonate given to the EDTA solution at 10 ml/hour. The Zn/Mg carbonate precipitation is extracted & processed with purified water and alcohol to get rid of contaminants like EDTA and the original reaction mechanism. Carbonic acid predecessor are created by dehydrating and processing wet precipitate in an agate mortar. Bones decompose into oxide when burned to the required temperature, which is the precursor of cru. The heat treatment rates for each system are established by energy dispersive & asymmetric thermal decomposition. To boost the mg contents of the specimens, the transition metal nano-composites test results created in this way were given the designations ZSM1, Z4M2, • Z3M3, Z2M4, and Z1M5. These IDs shall be utilized going forwards.

Results and discussion

Structural characterization

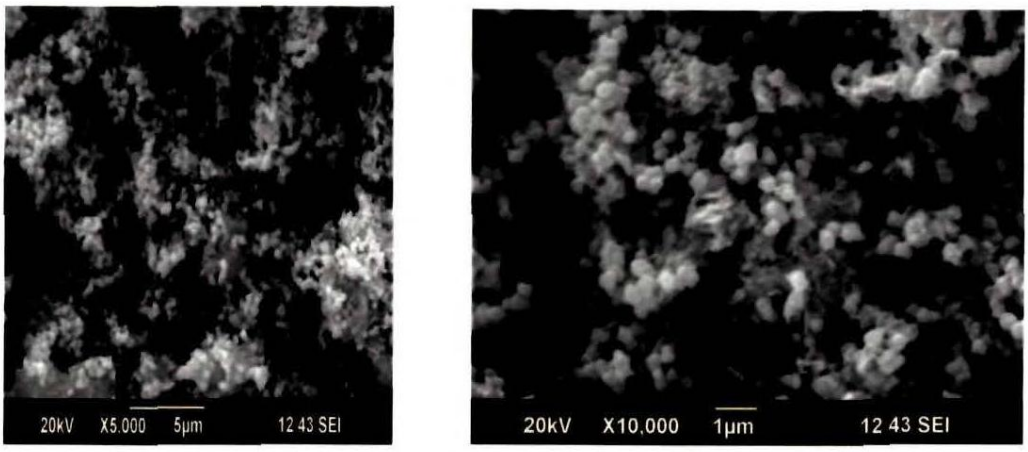

Figure 1: SEMs Pictures of the ZnO nanoparticles synthesize

EDAX of the powder (fig 2 and table 1) verifies Zinc Oxide nanoparticle production. The resulting nanoparticles are nearly rounded in form and homogenous in composition. The findings of EDAX demonstrate that the sample lacks oxygen.

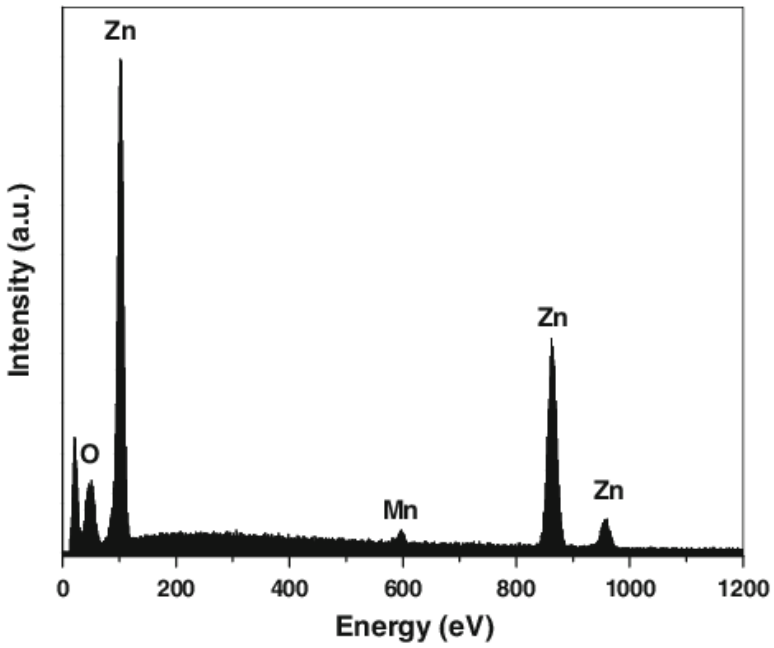

Figure 2: EDAX spectrum of Zinc Oxide nanoparticles

Fig 3 shows the structure characterized by X-ray diffraction. Identification of the lattice planes and comparison of the measured values with those stated in JCPDS Card No. 79-0208 reveal a high degree of agreement.

Table 1: Outcome of EDAX evaluation showing the percentage of Zn and 0 in the trial

Element	Mass (%)	Atom (%)
OK	6.68	22.62
Zn K	93.34	77.38
Total	100	100

Table 2: The lattice constants and interplanar distance in comparison with reported values

2θ	FWHM	Size Of Particle	Interplanar Distances			hkl	Lattice Parameter		Micro Strain (10^{-3})	Dislocation Density (10^{16})
			d_{obs}	d_{jcpds}	d_{diff}		A	B= c		
31.17	0.56	15	2.95	2.83	0.050	100	3.4	-	3.83	0.48
33.80	0.48	18	2.76	2.61	0.050	002	-	5.4	3.01	0.35
35.65	0.48	18	2.62	2.49	0.047	101	3.4	5.3	2.84	0.34
47.01	0.96	9	1.94	1.92	0.015	102	3.4	5.3	4.20	1.27
56.08	0.96	9	1.74	1.64	0.007	110	3.3	-	3.43	1.17
62.176	0.80	11	1.50	1.49	0.020	103	3.3	5.3	2.53	0.77
67.36	0.64	15	1.49	1.39	0.006	112	-	-	1.83	0.47

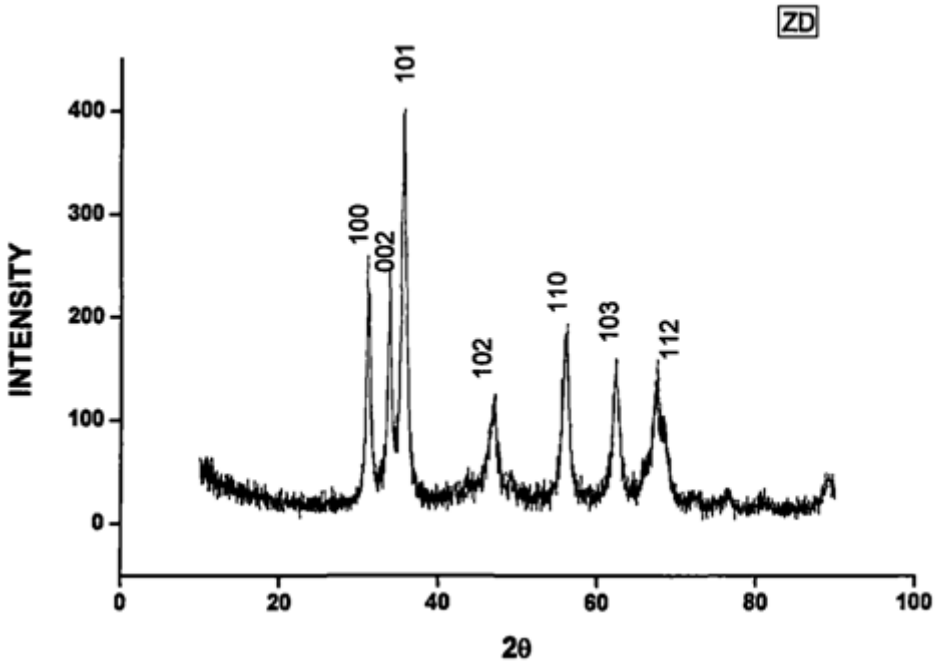

Figure 3: XRD spectrum of sample ZD

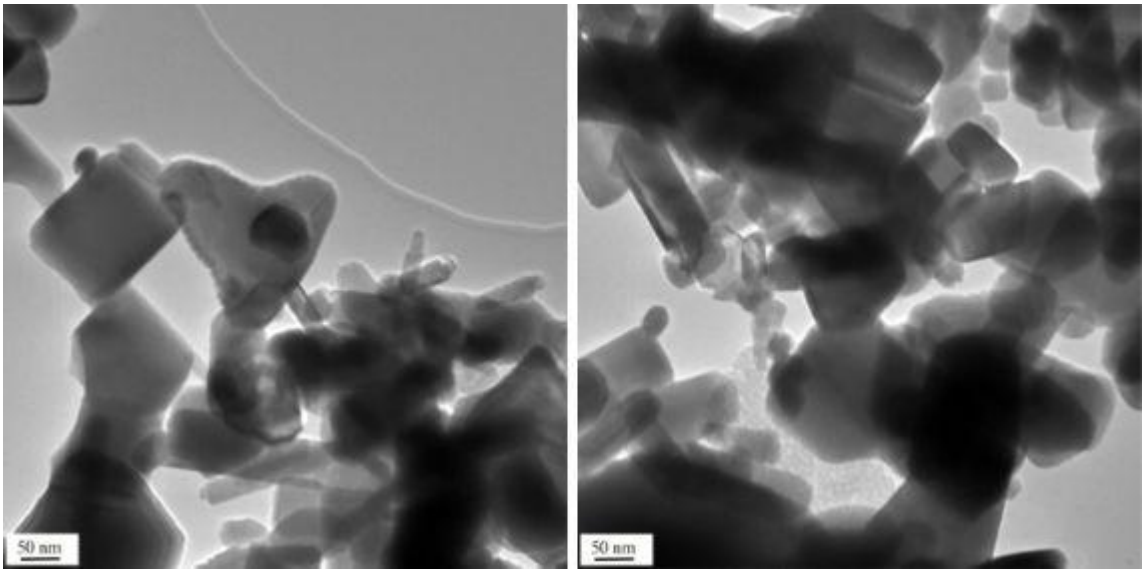

Figure 4: TEM images of ZoO nanoparticles synthesized using DRNA

The diffraction pattern data are in Table 2. The precipitate's crystal phase is identified by comparing X-ray diffraction spectra to JCPDS data. Figure 8.3 depicts distinct peaks were in high-quality accordance with Znic Oxide (1 00), (002), (1 01), (1 02), (11 0), (1 03), (200), (112), and (201). The estimated lattice parameter values, (a=3.303777 A0, b=c=5.25255 A0), are identical to the reported values (a=3.264 A0, b=c=5.219 A 0). The sample's diffraction peaks and the results stated on card no. 75-1533 are quite similar. The TEM images (Figv4) reveal molecular weights from 8nrn to 22 nm. Particle size is smaller than when topping with EDT A.

FTIR

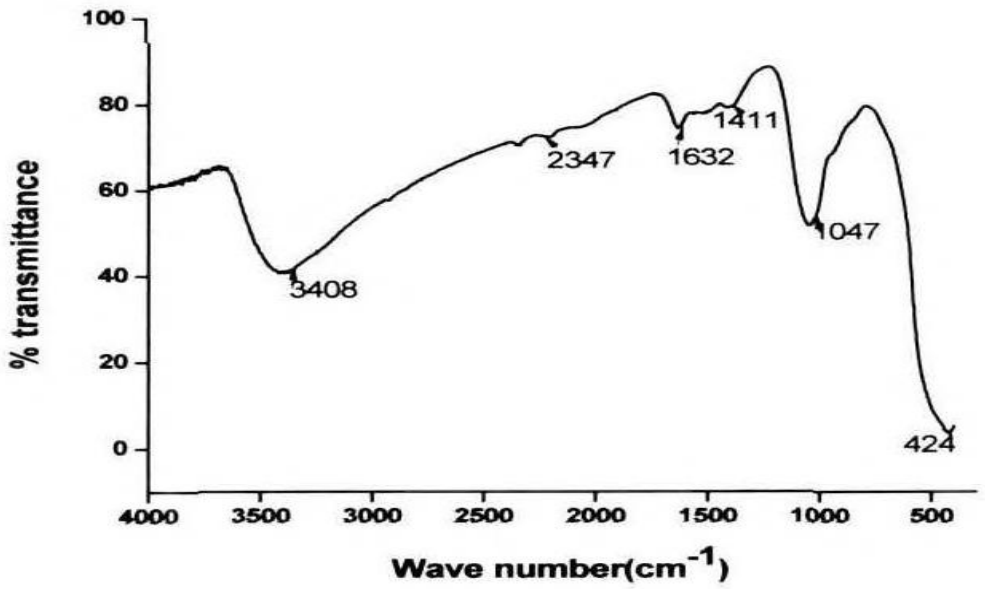

Figure 5: FTIR spectrum of ZoO nanoparticles

The FTIR spectra of synthetic nanoparticles containing zinc oxide are shown in fig 5. The band gap at 3408 cm-1 is an asymmetric OH bond stretch, while the band at 234 7 em -I obstructed aqueous valence resonance. The bands in the region of 1632 em –I show the existence of a carbonyl group; in this case, the band may be caused by C=O stretching in the monomer, but the group at 104 7 cm-1 is caused by C-0 stretching vibration. These bands show that there is some carbon-containing material present. The bands between 1400 em-I and 424 cm-1 are caused by cellulose fibers. Oxygen-zinc ion interactions create the band at 424 cm-1.

UV-Visible spectroscopy

UV-Vis spectral data of both specimens are comparable with peak shift. Instead of directly transferring absorption maximum wavelengths to the band gap, plot (ahu)2 against h and extend the linear component to the X axis. The Tauc plot for the nanomaterials Zinc Oxide is shown in fig 6. The band gap for the zinc oxide nanoparticle as it was generated is 3.625 eV, while the band gap for the sample after 700 °C annealings is 3.58 eV.

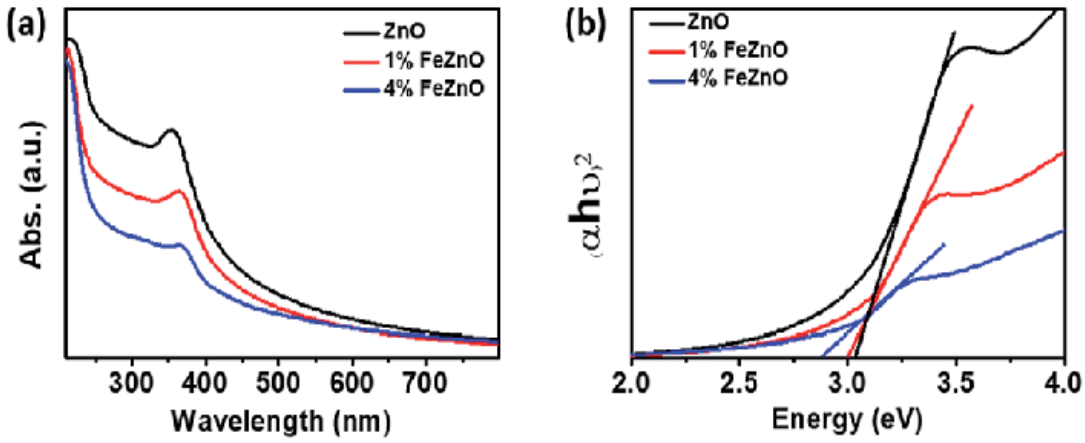

Figure 6: a) UV Absorption graph, b) Tauc plot for the determination of band gap

Photo luminescent emissions

Both inherent and extrinsic crystallographic flaws affect a semiconductor's optical characteristics. Defects may be caused by vacancies, interstitial atoms, or other factors.

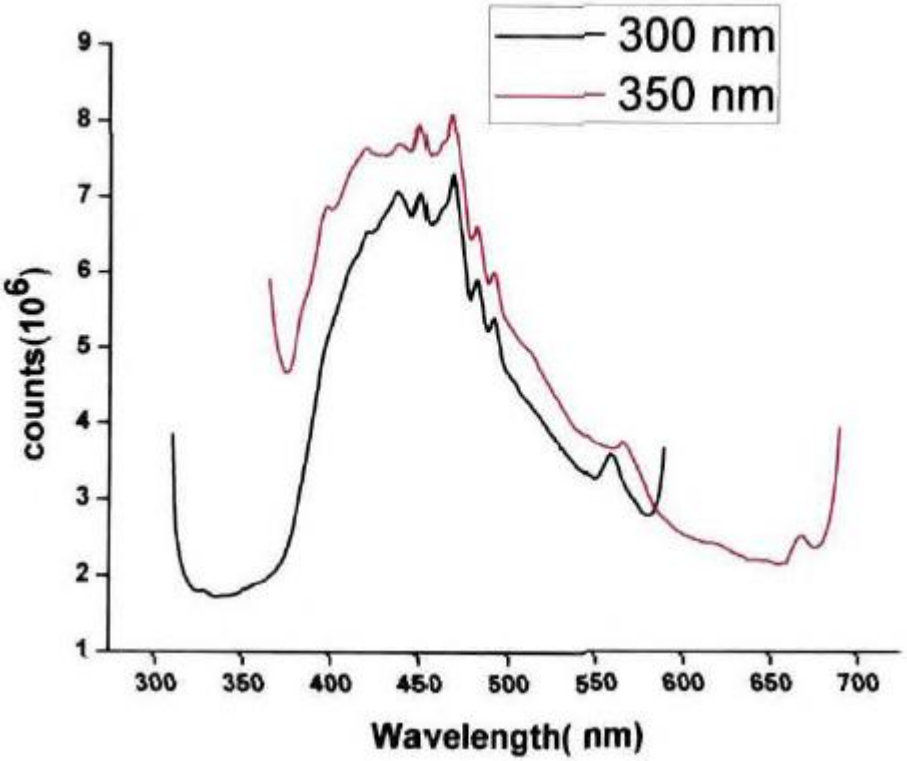

Figure 7: Photoluminescence spectrums of ZnO nanoparticles

If contaminants are included, the flaws are extrinsic. When a defect simply consists of the host atomic, it is referred to as an internal electron. Intrinsic optical recombination occurs between conduction-band electrons and valence-band holes. Both intrinsic and extrinsic point flaws provide ZnO fluorescence.Typically, a wide secretion band and a strong ultraviolet (UV) secretion band are seen. Most often, the transition combination of free excitation energy in the vicinity of ZnO's band-edge is blamed for the UVs emission spectrum. Deep-level flaws in ZnO cause the visible (420-750 nm) emission, band. Deep-level ZnO flaws alter its optical and electrical characteristics. By adjusting the number and kind of faults present in semiconductors, these qualities may be altered and controlled. The (DLE band in ZnO has been linked to VO [25]. Oi [26] VZn [27],Zuni,Oxygen anti Substitution Cu and Li [28-30] may also cause deep level emissions. The photoluminescence spectra (Fig 7) of nanostructured Zinc Oxide generated in this approach reveal a wide and strong emissions band in the blue region (420 nm -470 nm) with a modest emission at the spectral range. The resulting spectra don't include any further notable peaks. When the excitation wavelength was raised to 350 nm, the peak characteristics stayed the same. The spectrum is largely independent of excitation wavelength, showing nanoparticle homogeneity. ZnO emits blue light by moving from near the CB to deeper accepting areas. The luminescence absorption bands were the crystalline failure features.

Conductivity studies

The nano-structured molecule's DC conductance remains practically constant with rising temperatures till 383 K. (Fig 8). The fluctuation of log a Vs. 1000/T for de conductance and ac conductance at the lowest frequency is exposed in Figs 9a and 9b. The activate function from de experiments is 0.6257 eV while the activation energy from ac conductivity studies at a short wavelength is 0.7837 eV. Low activation increases or ac conduction at lower frequency occurs because the conduction method involves fewer mobile ions. Comparing the activation energy to that of Zinc Oxide nanoparticles made using EDT A, it is discovered to be higher.

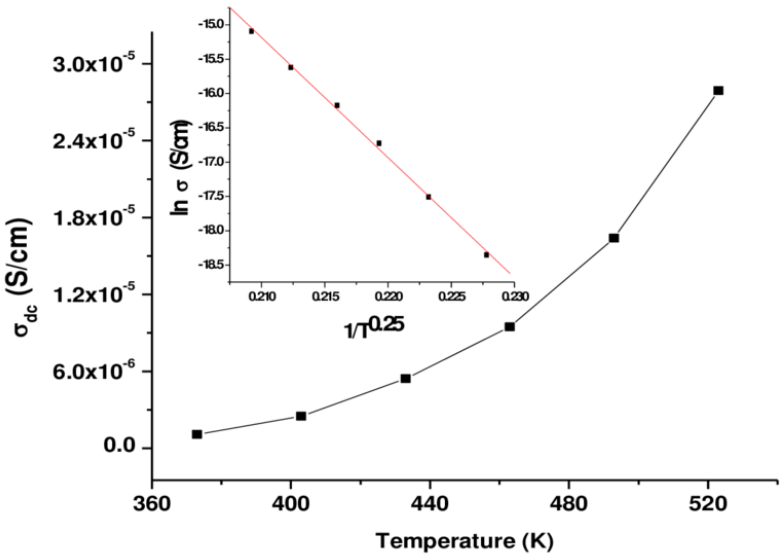

Figure 8: Variation of DC conductivity with temperature

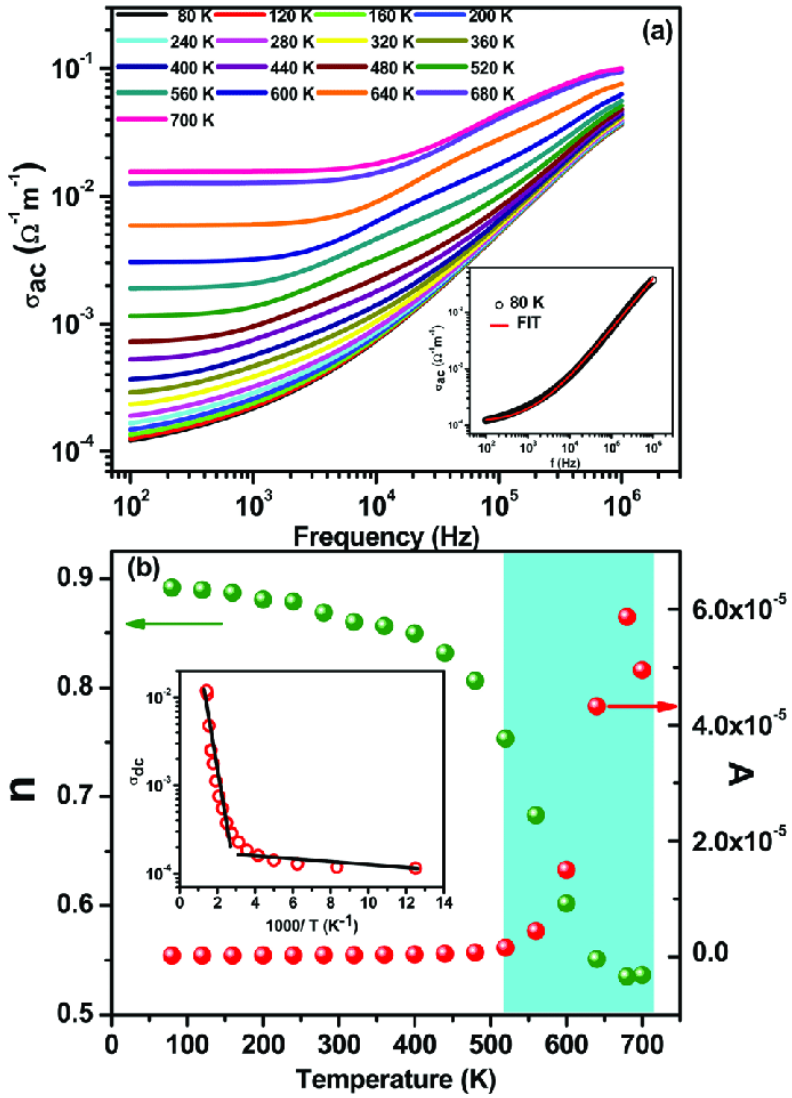

Figure 9 a) Arrhenius plot of DC conductivity b) Arrhenius plot of AC Conductivity

The fluctuation of Conductivity with temperatures at various frequencies is seen in graph 10. It demonstrates how conductivity initially rises, then reaches the maximum value before falling. At high

temperatures, the value essentially stays the same before increasing past 403 K. At all wavelengths, the basis of conductivity's modulation with temperatures is the same.

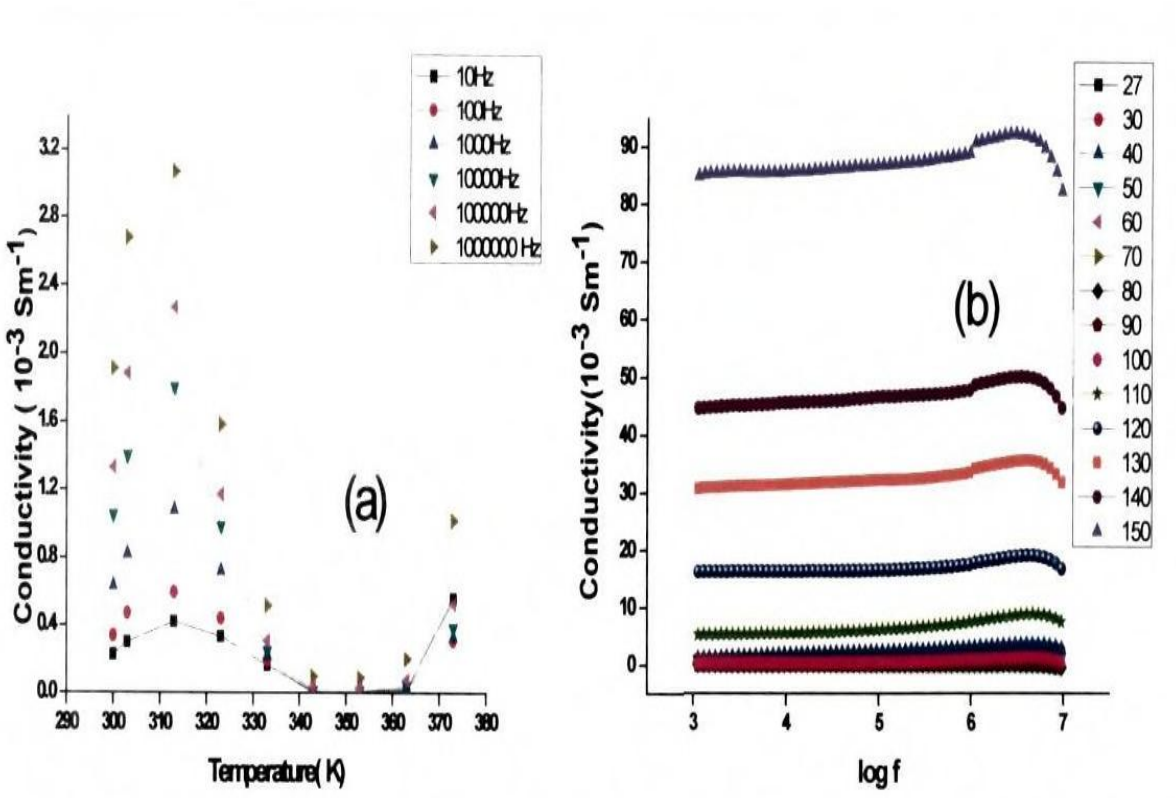

Figure 10: Variation of Conductivity a) with temperature b) with frequency

Dielectric Studies

The dielectric constant changes with temperature (fig 11a) at different wavelengths. Variation in dielectric constant with temperatures is the same for all frequencies, despite various ranges. The dielectric constant rises first, reaches its peak, and then falls. At elevated temp, dielectric loss is constant. With temperature rises, it is discovered that the high dielectric drops and shifts higher (fig 11 b)

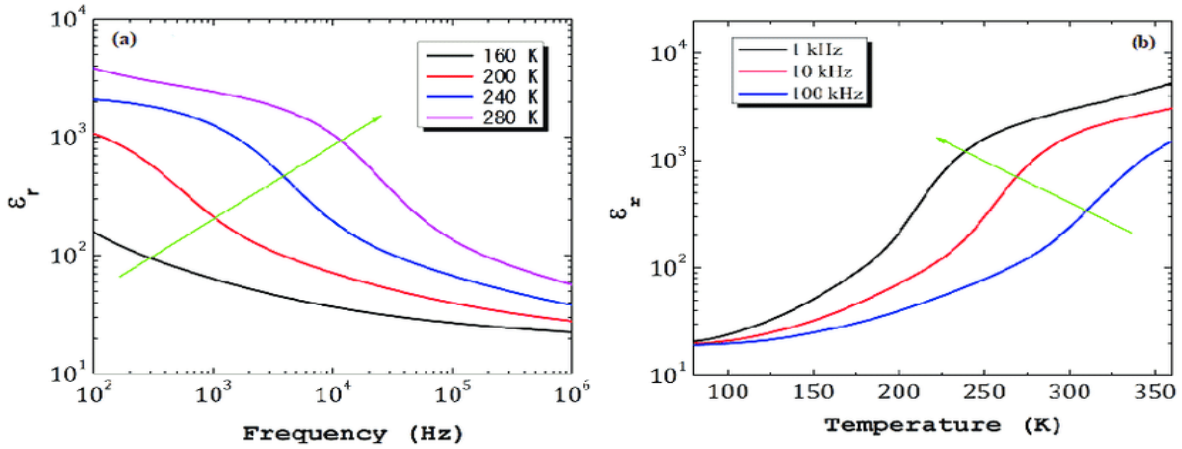

Figure 11: Variation of Dielectric permittivity a) frequency b)temperature

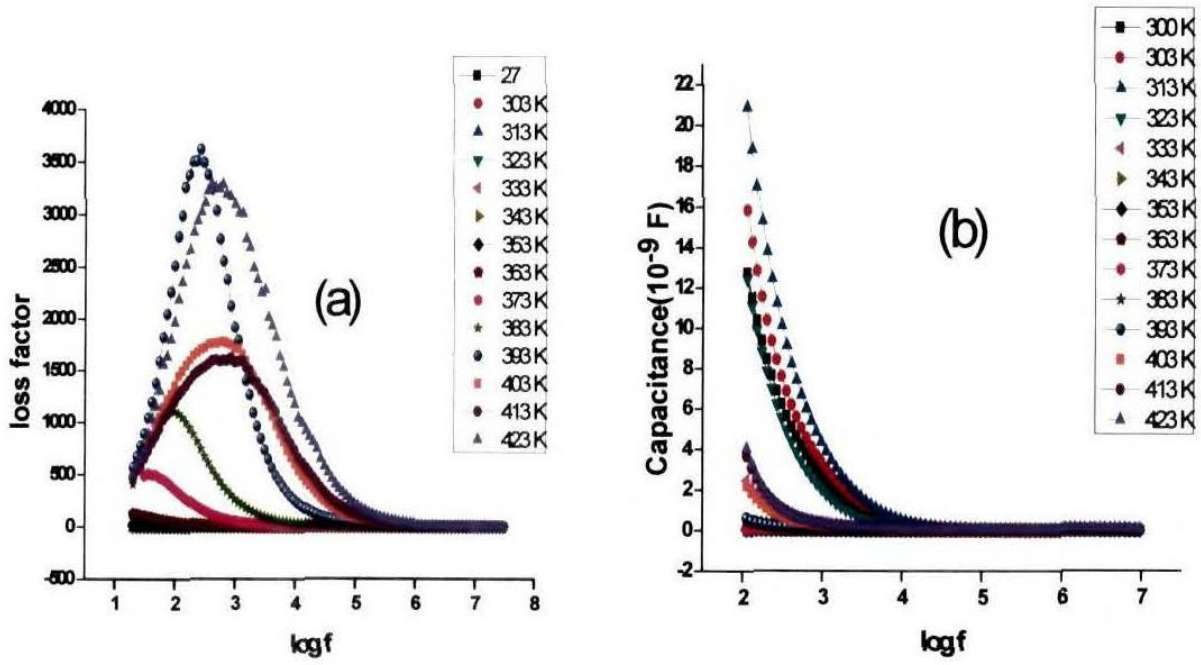

Figure 12: Variation of a) loss factor using log f and b) capacitance with log f

The lattice's energy loss as a result of the polarization effects that result from the introduction of an electric field is measured by the loss factor. exhibit fig 12 shows how the loss factor varies with frequency and temperature. The graph shows several relaxation processes in the material and temperature-dependent polarization.

Cole -Cole analysis

The Cole-Cole technique of analysis, together with its theoretical underpinnings and practical applications, is dissected in great length in Chapter 5. The material underwent a Cole- Cole analysis between 333 K and 373 K. Semi circles with centers below the real axis imply numerous relaxation mechanisms in the material's dipoles. Thus, a relaxing time is distributed from around the median relaxation time, as seen in Table 3. The optical dielectric constant fell first but subsequently grew quickly. A comparable fluctuation was seen in the static dielectric constant. Fig 13 displays the Cole-Cole graphs created for the zinc oxide nanoparticle at various temperatures. The spreading factor, refractive and static dielectric constants and active suspension are presented in Table 3. In the substance, settling time spreads out as the temperature rises. Temperature-related small fluctuations were seen in the optical dielectric constant (e∞) and static dielectric constant. The typical settling time is 1 o-8s, and its fluctuation may be used to find acceleration.

Table 3: Dispersion parameters of Zinc Oxide nanoparticles prepared using DRNA

Temp	α	ϵ_{max}	τ_0*10^{-8} s	τ *10^{-8} s	ϵ_∞	ϵ_s
333	0.13	6.14	1.96	1.56	8.89	23.626
343	0.47	2.81	6.55	5.20	7.51	19.86
353	0.47	2.67	6.43	5.12	7.60	19.44
363	0.35	0.35	2.75	2.31	8.88	17.23
373	0.21	13.97	1.68	1.26	12.76	51.20

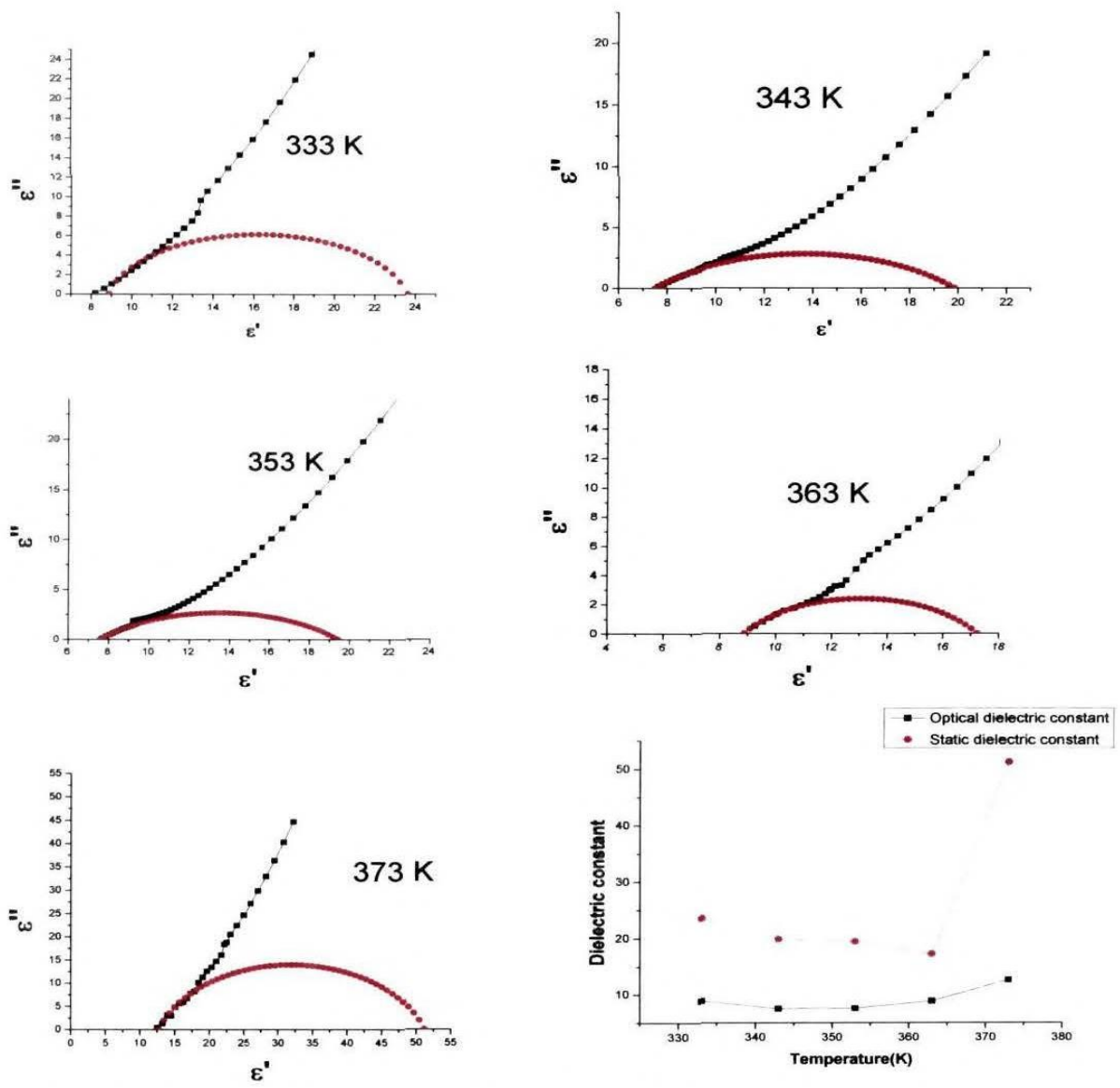

Figure 13: Cole -Cole plots at different temperatures and variations in optic and static dielectric constants

Conclusion

The green synthesis process, which makes use of DRNA, was effective in producing nanoparticles of ZnO. The TEM indicates that nanoparticles were uniform in shape and most were 13 nm in size. We investigate the optical spectrum gap and luminous characteristics. A 3.7 eV bandgap is discovered. Comparing the structural, optical, and electrical characteristics of nanoparticles produced using DRNA to those produced with EDTA. The structure has altered, and the luminous characteristics have also been modified. The wide and strong blue-violet emissions bands make them suited for blue dozing applications. Standardization and improved circumstances exist. The yield of high-quality nanomaterials is produced by selecting the appropriate molarity. According to the differential thermal study, the bicarbonate predecessor decomposes around 450° C for ZnO, MgO, and (ZnO/MgO), and 350° C for ZnO/CdO. The low temperature exothermic breakdown of the carbon material included in the precursor powdered lowers the melting temperature required for the creation of tiny particles in this mixed oxide environment.

Reference

1. Abdeen A. M., "Dielectric behaviour in Ni-Zn ferrites", J. Magnetism and Magnetic Material, vol192, 1, (1999), 121.

2. 2. Ahmed M. A. and Elhiti M. A., "Electrical and Dielectric-Properties of Zn o.s Co 0.2 Fe204", Journal de Physique, 111, 5, (1995), 775.
3. Alexandrov A. S., Phys Rev Lett., 95, (2005), 259704.
4. Alexandrov A.S. and Mott N.F., Phys Rev. Lett, 71, (1993), 1075.
5. Ali H.A., Iliadis A. A., Mulligan R. F., Cresce A. V. W;, Kofinas P. and Lee U., "Properties of self-assembled ZnO nanostructures", Solid State Electron, 46, (2002), 1639.
6. Alivisators A.P., "Semiconductor Clusters, Nanocrystals, and Quantum dots", Science 271, (1996), 933.
7. Allan G., Delerue C. and Lannoo M, "Quantum confinement in the Si-III (BC-8) phase of porous silicon", Appl. Phys. Lett, 70, (1997), 2437.
8. Allan G., Delerue C.and Lannoo M, "Quantum Confinement in AmorphousSilicon Layers", Applied physics letters, 71, (1997), 1189.
9. Khan A., Kordesch M.E., "Synthesis of novel zinc oxide microphone-like microstructures", Mater Lett 62, (2008), 230.
10. Kim J.S., Kuk E., Yu K.N., Kim J.H., Park S.J., Lee H.J., Kim S.H., Park Y.K., Park Y.H., Hwang C:Y., Kim Y.K., Lee Y.S., Jeong D.H., Cho M.H., "Antimicrobial effects of silver nanoparticles", Journal ofNanomedicine 3(1), (2007), 95.
11. Kim S. , Seong S. Y., Cho C. R., "Structural reconstruction of hexagonal to cubic ZnO films on Pt/Ti/Si02/Si substrate by annealing", Appl. Phys. Lett. 82, (2003), 562.
12. Kittel C., Introduction to Solid State Physics, Seventh edn, Wiley Eastern Limited, (1996) ,29.
13. Ashrafi A.and Jagadish C., "Review of zinc blende ZnO: Stability of metastable ZnO phases", J. Appl. Phys., 102, (2007), 071101
14. Asif M. H, Ali S.M. U., Nur 0., Willander M., Brfummark C., Striilfors P., Englund U. H, Elinder F., Danielsson B., "Functionali:Zed ZnO-nanorod-based selective electrochemical sensor for intracellular glucose", Biosens. Bioelectron. 25, no. 10, (2010), 2205.
15. Asif M. H., Fulati A., Nur 0., Willander M., Brannmark C., Stralfors P., Borjesson S. I., Elinder F., " Functionalized zinc oxide nanorod with ionophore-membrane coating as an intracellular Ca2+ selective sensor", Appl. Phys. Lett., 95,(2009), 023703.
16. Preethi, P., Asokan, R., Thillaiarasu, N., & Saravanan, T. (2021). An effective digit recognition model using enhanced convolutional neural network based chaotic grey wolf optimization. Journal of Intelligent & Fuzzy Systems, (Preprint), 1-11.
17. Bandyopadhyay A. K., "Nanomateials" New Age International (P) Ltd (2007)
18. Banwell C. N. and McCash E. M.," Fundamentals of molecular spectroscopy", Tata McGraw Hill, 4 edition, 1994.
19. Baockelmann H.K., Schlecht R.G., "Raman scattering from microcrystals of MgO", Phys. Rev. B, 10, (1974), 5225.
20. Barati M.R., Ebrahimi S.A.S., Badiei A., Non-crystallineSolids, 354(47-51), (2008), 5184.
21. Bates C. H., White W.B., Roy R., "New High-Pressure Polymorph of Zinc Oxide", Science 137, (1962), 993.
22. Binns Chris, "Introduction to Nanoscience and Nanotechnology", John Wiley & Sons, 2,(2010)
23. Ma Dewei, Ye Zhizhen, Wang Lei, Huang Jingyun and Zhao Binghui, "Deposition and characteristics of CdO films with absolutely (200)-preferred orientation",, Materials Letter, 58 (2004),128.
24. Manohar B., Reddy V. R., Reddy B. M., Synth Comm, 28(17), (1998), 3183.
25. Mansfield R., in Hopping Transport in Solids, edited by M. Pollak and B. I. Shklovskii North-Holland, Amsterdam, (1991), 349.
26. Mee C. D., Jescheke J.D., "Single-Domain Properties in. Hexagonal Ferrites," J Appl. Phys. 34, (1963), 1271.
27. Meyer B. and Marx D., "Density-functional study ofthe structure and stability ofZnO surfaces", Phys. Rev. B 67, (2003), 035403.

28. Meyer B.K., Alves H., Hofmann D.M., Kriegseis W., Forster D.,Bertram F.,Christen J., Hoffmann A:, Straburg M., Dworzk M., Haboeck U.,Rodina A.V., "Bound exciton and donor-acceptor patr recombinations in ZnO",Phys.Stat.Sol. (b) 241, (2004), 231.
29. Mohammed E. M., Anantharaman M. R.," Fabrication of Conductivity Cell and Automation for the Measurements of Permittivity and a<? Conductivity": J. Instrum. Soc. India 32 (3) ,(2002), 1657.
30. Mott N. F., and Davis E. A., Electronic Process in Non-Crystalline Materials ~Oxford, UK, (1979).